Tuning from blue to magenta the up-converted emissions of YF_3:Tm^{3+}/Yb^{3+} nanocrystals

Marta Quintanilla,*[a] Nuria O. Núñez,[b] Eugenio Cantelar,[a] Manuel Ocaña[b] and Fernando Cussó[a]

Received 14th September 2010, Accepted 5th November 2010
DOI: 10.1039/c0nr00676a

Monodisperse YF_3:Tm^{3+}/Yb^{3+} nanocrystals have been synthesized to explore the visible up-converting properties under near infrared (975 nm) excitation. It has been found that the nanoparticles exhibit intense red up-converted emissions, in addition to the characteristic UV and blue Tm^{3+}-bands. It is demonstrated that, by carefully selecting Tm^{3+} and Yb^{3+} contents, the relative intensity of the different emissions can be changed producing an overall emission colour that can be tuned from blue to magenta.

Introduction

Up-conversion phosphors emit visible light after excitation by lower energy photons, usually in the near infrared spectral range. They have potential applications in different fields of science and technology, including luminescent displays, optoelectronic devices or lasers and amplifiers.[1–3] Recently, a great interest has been devoted to their use in infrared (IR) and visible imaging for biological research and medical diagnosis,[4–7] because of their important advantages when compared to the traditional bio-labels such as organic dyes, semiconductors or metallic nanoparticles. For example, the up-conversion mechanisms are favourable compared to traditional down-conversion ones due to the higher penetration depth of light achieved in tissues under IR excitation wavelengths. Moreover, this excitation scheme also accounts for the lower photo-damage to living organisms, and the possibility of obtaining a higher spatial resolution and weak auto-fluorescence from cells or tissues.[8,9] Additionally, it is possible to obtain nanophosphors with low toxicity, which is also one of the main points of interest in comparison with other bio-labels.[10,11]

Rare-earth (RE) based up-conversion nanophosphors are based on the combination of ion pairs acting as sensitizers–activators that allow a variety of excitation–emission choices.

Among all the studied lanthanide doped materials, the fluorides family ($NaYF_4$, LaF_3, YF_3, …) are the materials considered as the best hosts for efficient up-conversion,[12] favoured by the low phonon energy of these materials, which enhance the luminescence efficiency of RE dopants.[13] Therefore, a great research effort has been done to develop synthesis routes to obtain uniform nanoparticles of those materials,[14–18] and to study the relationship between shape, size and dopant concentration with the optical properties.[19,20]

In particular, Yb-activated materials are extensively used because of its convenient near IR absorption band, accessible by commercially available diode-lasers, and its efficient sensitization of several emitting rare earths (Er^{3+}, Tm^{3+}, …). Depending on the particular ion used as activator different emissions can be obtained: Er^{3+} ions are selected as a standard green and red emitters, while Tm^{3+} ions are chosen as blue emitters.

Along this line, there are a number of recent studies devoted to Yb^{3+}/Tm^{3+} co-doped fluoride hosts,[16,21,22] including YF_3:Yb^{3+}/Tm^{3+} nanoparticles.[17,23–29] Nevertheless, in this material the emissions seem to be restricted to the high energy side of the spectrum. Enhanced UV and blue up-converted emissions have been reported[23–26] but they exhibit negligible emissions in the lower energy spectral range. At variance, it has been recently reported[19] for monodisperse β-$NaYF_4$:Yb^{3+}/Tm^{3+} the appearance of sizeable red emissions, which have not been observed before in YF_3. It is also noteworthy that the YF_3:Yb^{3+}/Tm^{3+} synthesis procedures reported in previous works led, in most cases, to particles with irregular shape and heterogeneous size, both in the nanometre or micrometre size range. In fact, to our knowledge, only the procedure developed by Wang *et al.*[27] (based in the use of microemulsions), led to truly uniform Tm^{3+}-based nanophosphors with octahedral shape and a mean size of about 100 nm.

In the present work we have synthesised YF_3:Yb^{3+}/Tm^{3+} uniform nanophosphors with rhombic shape and reported, for the first time, that they present efficient red up-converted emission, in addition to the well known UV-blue emissions. Furthermore the overall emission characteristics can be controlled and tuned by changing the relative concentration of the RE-dopants. The bright up-conversion emissions, both in the UV-blue and the red spectral region, make them suitable for biological applications.

For the synthesis of the uniform YF_3:Tm^{3+}/Yb^{3+} nanocrystals with rhombic shape and different doping levels, we have used a simple and environmentally friendly procedure, previously developed by us to produce YF_3 down-conversion (Eu^{3+} or Tb^{3+} doped) phosphors,[15] which has been properly modified for the preparation of Yb^{3+}/Tm^{3+} co-doped YF_3.

Experimental section

Reagents

Yttrium(III) acetate (YOAc, $Y(CH_3COO)_3 \cdot XH_2O$, Aldrich, 99.9%), thulium(III) acetylacetonate ($Tm(CH_3COCHCOCH_3)_3$,

[a]*Departamento de Física de Materiales (Módulo 04), Universidad Autónoma de Madrid, C/Francisco Tomás y Valiente, 7, 28049 Madrid, Spain. E-mail: marta.quintanilla@uam.es; Fax: +34 91 497 85 79; Tel: +34 91 497 24 50*
[b]*Instituto de Ciencia de Materiales de Sevilla, CSIC-US, Américo Vespucio 49, Isla de la Cartuja, 41092 Sevilla, Spain. E-mail: mjurado@icmse.csic.es; Fax: +34 95 446 06 65; Tel: +34 95 448 95 33*

Alpha Aesar, 99.9%), and ytterbium(III) acetylacetonate ($Yb(CH_3COCHCOCH_3)_3$, Alpha Aesar, 99.9%) were selected as Ln precursors. 1-Butyl-3-methylimidazolium tetrafluoroborate ([BMIM]BF_4, $C_8H_{15}BF_4N_2$, Fluka, 97%) was used as a fluoride source and ethylene glycol (EG) (Fluka, 99.5%) or diethylene glycol (DEG) (Aldrich, 99%) as solvents. All chemicals were used as-received.

Nanoparticles synthesis

Different yttrium fluoride based phosphors containing variable Yb^{3+} (from 1 mol% up to 30 mol%) and Tm^{3+} (from 0.1 mol% to 5 mol%) contents were synthesized using the following standard procedure:[15] proper amounts of the rare-earth precursors were dissolved in ethylene glycol under magnetic stirring, heating the vial at ~100 °C to facilitate the dissolution process. These solutions were cooled down to room temperature after which, the desired volume of [BMIM]BF_4 was admixed keeping the magnetic stirring. The final solutions (total volume = 10 cm^3) were then aged for 15 h in tightly closed test tubes using an oven preheated at the selected temperature.

After ageing, the resulting dispersions were cooled down to room temperature, centrifuged to remove the supernatants and washed, twice with ethanol and once with double distilled water. The powders were then dried at 50 °C and annealed for 20 min at 400 °C. In the case of YF_3:Er^{3+}/Yb^{3+} nanoparticles prepared by a similar procedure, this treatment has been proven to be adequate to eliminate residual OH^- groups, resulting in enhanced fluorescence properties, while preserving the size and shape of the nanocrystals.[30]

Instrumentation

The shape of the nanoparticles was examined by transmission electron microscopy (TEM, Philips 200 CM). For this, a droplet of an aqueous suspension of the samples was deposited on a copper grid coated with a transparent polymer and dried. The particle size distributions were obtained from the micrographs by counting several hundreds of particles.

The composition of the precipitated particles was assessed by energy dispersive X-ray analysis (EDX, Philips DX4) coupled to the TEM microscope. In order to obtain structural information on the prepared nanoparticles, we used X-ray diffraction (XRD, Siemens D501). Unit cell parameters were measured by Rietveld refinement of the XRD data using the X'Pert HighScore Plus software.

The optical measurements for powdered pressed samples were performed using a JENOPTIK laser diode source at 980 nm to excite the Yb^{3+} ions with different excitation powers. The visible Tm^{3+} luminescence was dispersed by using an ARC Spectrapro 500-I monochromator and then detected with an ultraviolet enhanced photomultiplier tube (Thorn Emi QB9558).

In order to achieve reproducible and comparative luminescence spectra, all the data have been taken using a standard experimental arrangement, including specially design sample holders. They were constructed using a 1 mm thick PMMA spacer with a 2 mm diameter circular opening, enclosed by two microscope slide covers. The nanopowders were introduced filling the cavity, which was placed in a fixed mounting on the top of a micrometre stage, in order to optimize the luminescence signal.

The diode laser beam was limited by a diaphragm assuring that the excitation area was smaller than the exposed sample area. The sample holder can be removed and replaced into this arrangement without altering the geometry.

Results and discussion

Nanoparticles synthesis and structural characterisation

The particles synthesised by the described procedure were highly uniform and presented a rhombic-like morphology and a mean size (125 × 55 × 25 nm) in the nanometre range (Fig. 1).

Fig. 2 shows the EDX spectra measured for a sample with composition YF_3:Yb^{3+} (10%)/Tm^{3+} (2%) chosen as a representative example. As observed, the main peaks corresponding to F, Y, Yb and Tm were detected confirming the incorporation of the doping cations to the YF_3 nanoparticles. It should be also noted that the EDX spectra recorded for several single particles were almost identical, pointing towards a high degree of chemical homogeneity in the sample, at least at the particle level.

The XRD pattern of the samples indicated that the nanoparticles were well crystallized and consisted of orthorhombic YF_3 (JCPDS file no. 32-1431), as illustrated in Fig. 3 for the sample shown in Fig. 1. Finally, the comparison of the unit cell parameters measured for a nanophosphor sample having a high Tm^{3+} content (for a better observation of the changes) with those of an undoped sample (Table 1) clearly manifests the formation of a solid solution between the doping cations and the YF_3 host. Thus, a contraction of the YF_3 unit cell was detected for the phosphor nanoparticles which is in agreement with the smaller size of Tm^{3+} (0.87 Å) and Yb^{3+} cations (0.858 Å) when compared with that of Y^{3+} (0.893 Å).[31]

Optical characterization

Ytterbium ions are used as sensitizers of other lanthanide ions because of its IR absorption, extending from 920 nm and 980 nm, which populates the only excited state of Yb^{3+} ($^2F_{7/2} \rightarrow {}^2F_{5/2}$ transition). Following this scheme, Tm^{3+} ions can be excited by a series of non-resonant energy transfer mechanisms that are described in the literature.[32–34] In Fig. 4 the generally accepted processes that generate UV and blue emissions in Tm^{3+}/Yb^{3+} systems after IR excitation are shown. As it can be seen, once the sensitizers are populated, a first energy transfer process can take

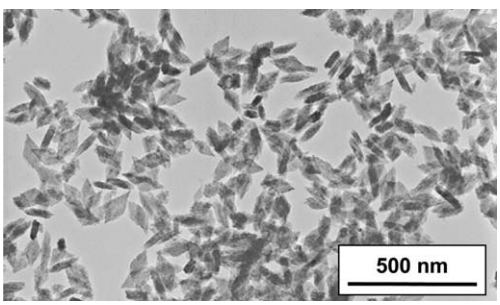

Fig. 1 TEM image of the YF_3:Yb^{3+} (10%)/Tm^{3+} (2%) sample showing the homogeneity and size of the particles.

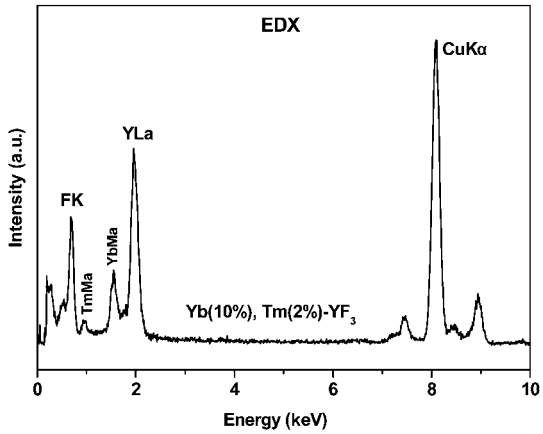

Fig. 2 EDX spectrum for the YF_3:Yb^{3+} (10%)/Tm^{3+} (2%) sample. The most intense peak for each element has been labelled.

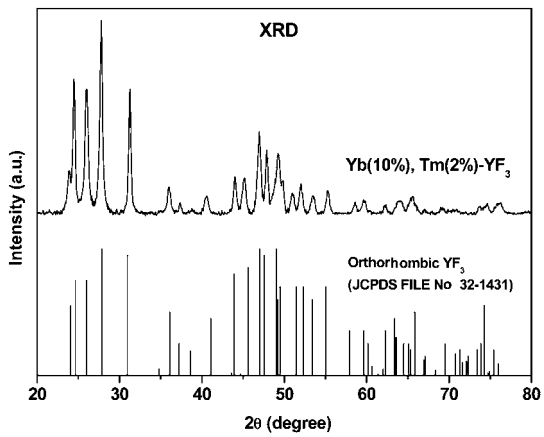

Fig. 3 X-Ray diffraction pattern for the YF_3:Yb^{3+} (10%)/Tm^{3+} (2%) sample. The reference pattern for orthorhombic YF_3 (JCPDS 32-1431) is also included.

place following the mechanism $^2F_{5/2} \rightarrow {}^2F_{7/2}$ (Yb^{3+}):$^3H_6 \rightarrow {}^3H_5$ (Tm^{3+}). $^3H_5$ level is then relaxed mainly by a non-radiative way populating the lower lying level of thulium $^3F_4$. Then, a second energy transfer process involving both Yb^{3+} and Tm^{3+} ions can take place *via* the mechanism $^2F_{5/2} \rightarrow {}^2F_{7/2}$ (Yb^{3+}):$^3F_4 \rightarrow {}^3F_{2,3}$ (Tm^{3+}). The lower lying $^3H_4$ multiplet receives then some population from the non-radiative relaxation of $^3F_{2,3}$, allowing the occurrence of a third up-conversion process that populates the $^1G_4$ level: $^2F_{5/2} \rightarrow {}^2F_{7/2}$ (Yb^{3+}):$^3H_4 \rightarrow {}^1G_4$ (Tm^{3+}). All those up-conversion energy transfer processes are depicted in Fig. 4a.

It is possible a further step to populate an even higher energy level of thulium, $^1D_2$, although in this case the exact mechanism is

Table 1 Unit cell parameters and unit cell volume measured for a YF_3:Tm^{3+}/Yb^{3+} nanophosphor sample compared with those of the undoped YF_3 nanoparticles

	a/Å	*b*/Å	*c*/Å	*V*/Å^3
YF_3	6.347(1)	6.871(1)	4.432(1)	193.31
YF_3:Yb^{3+} (10%)/Tm^{3+} (5%)	6.310(1)	6.853(1)	4.445(1)	192.23

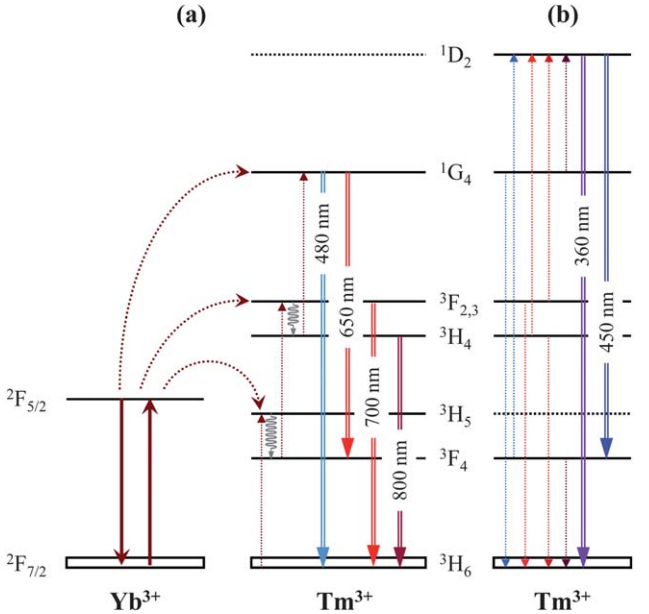

Fig. 4 Energy level scheme showing the different energy transfer processes responsible for the generation of UV and visible light emission in Tm^{3+}/Yb^{3+} systems after excitation at Yb^{3+} ions.

not yet fully elucidated. Different processes have been proposed to explain the way this level can be excited: on one hand, it has been proposed a fourth energy transfer involving Yb^{3+} ions as sensitizers and, alternatively, several $Tm^{3+} \rightarrow Tm^{3+}$ internal cross-relaxation processes have been invoked.[21,23,35,36]

The proposed fourth energy transfer, $^2F_{5/2} \rightarrow {}^2F_{7/2}$ (Yb^{3+}):$^1G_4 \rightarrow {}^1D_2$ (Tm^{3+}), is highly non-resonant, involving a large energy mismatch between the different transitions: $\Delta E \approx 3300$ cm^{-1}, so that it seems to be an unlikely process in a host with low phonon such as YF_3 ($E_{ph} \approx 514$ cm^{-1}).[13] Therefore, $Tm^{3+} \rightarrow Tm^{3+}$ resonant energy transfer processes ($^1G_4 \rightarrow {}^3H_6$:$^3F_4 \rightarrow {}^1D_2$; $^3F_{2,3} \rightarrow {}^3H_6$:$^3H_4 \rightarrow {}^1D_2$ and $^3H_4 \rightarrow {}^3H_6$:$^3F_{2,3} \rightarrow {}^1D_2$) seem to be more plausible mechanisms to populate $^1D_2$ energy level[21,23]. These processes have been depicted in Fig. 4b.

Then, after Yb^{3+} excitation, different Tm^{3+} multiplets are populated and it is possible to observe several emissions from the near ultraviolet to near IR spectral range. The emission spectrum, obtained after excitation at 975 nm (coincident with the maximum absorption cross-section wavelength of ytterbium ions in YF_3), is presented in Fig. 5. This particular example corresponds to nanoparticles with dopants concentration: [Tm^{3+}] = 2 mol%; [Yb^{3+}] = 20 mol% and it has been recorded in the spectral region between 300 nm and 900 nm. As it can be observed, there appear different bands in the ultraviolet, blue, red and near IR regions, which originate from the Tm^{3+} excited states: $^3H_4$, $^3F_{2,3}$, $^1G_4$ and $^1D_2$.

All the transitions have been labelled in the figure according to the general assignment of thulium emissions, and, for the sake of clearness, they are also depicted in Fig. 4 as double arrows. As it can be seen, the near IR emission, centred at ~800 nm originates from the $^3H_4 \rightarrow {}^3H_6$ transition, the emissions centred at ~650 nm and ~476 nm are both due to emissions from $^1G_4$ level ($^1G_4 \rightarrow {}^3F_4$ and $^1G_4 \rightarrow {}^3H_6$ transitions, respectively) and the emissions centred at ~450 nm and ~363 nm arise from $^1D_2$ level ($^1D_2 \rightarrow {}^3F_4$ and

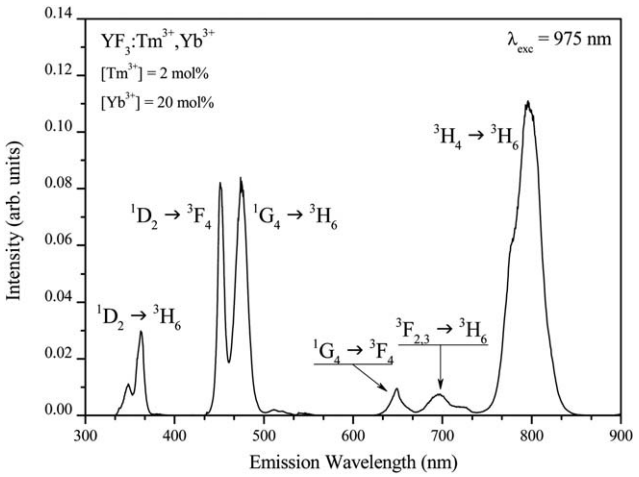

Fig. 5 Emission spectrum of a YF_3:Tm^{3+}/Yb^{3+} ([Tm^{3+}] = 2 mol%, [Yb^{3+}] = 20 mol%) sample under excitation at ytterbium ions.

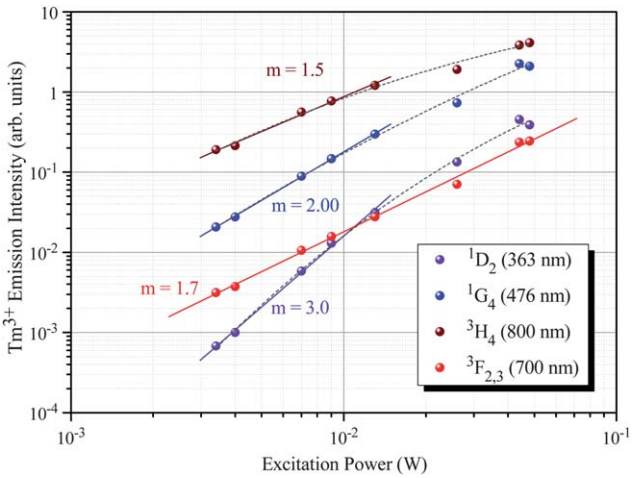

Fig. 6 Power dependency of the emission intensity of Tm^{3+} transitions that take place from different levels to the ground state, $^3H_6$. The full lines represent the fits made to obtain the slopes. The dotted lines are polynomial fits drown to guide the eye.

$^1D_2 \rightarrow {}^3H_6$ transitions, respectively). This spectrum is similar to that reported for different authors[16,21,24,26] although in this case a non-negligible red emission, at around 700 nm, ascribed to the $^3F_{2,3} \rightarrow {}^3H_6$ transition, is also clearly visible. This emission has been rarely observed in YF_3:Yb^{3+}/Tm^{3+} nanoparticles but its significance has been recently pointed out in $NaYF_4$:Yb^{3+}/Tm^{3+} nanoparticles.[19]

Information about the processes involved in the UC emissions can be achieved from the dependence of the intensity of the different emission bands as a function of the IR excitation power. This dependence brings information on the up-conversion mechanisms, as it is related to the number of photons needed for the successive up-conversion processes.[37]

In the simplest situation, the power dependence would indicate the number, *n*, of photons (UC-steps) involved in the process. Nevertheless, it is often found a saturation effect which reduces the experimental power dependence. In these cases the slope values provided by the emission intensity *versus* excitation power graph represent just a lower limit of the number of photons involved in the population process.[37]

The experimental power dependences of the up-converted Tm^{3+} emissions are presented in Fig. 6. As it can be observed in the figure, the power dependency deviates from linearity, indicating that some of the excited states involved are saturated. Anyway, in the low pump power regime, the intensity of the up-converted emissions exhibits a power dependence with slopes of 1.5 for $^3H_4 \rightarrow {}^3H_6$ transition, 2.0 for $^1G_4 \rightarrow {}^3H_6$ and 3.0 for $^1D_2 \rightarrow {}^3H_6$, represented by the continuous coloured lines in the figure. The red emission (700 nm) associated to the $^3F_{2,3} \rightarrow {}^3H_6$ transition follows a linear dependence with a slope 1.7 through all the power range used in this work.

As it has been indicated above, considering the evidence of saturation these power dependences represent the lower limit of the number of photons involved in the up-conversion mechanisms. Therefore, the experimental results are consistent with the mechanisms shown in Fig. 4, that suggest a two-photon process for $^3F_{2,3}$ and $^3H_4$ population, a three-photon process for $^1G_4$ emissions and, at least, a four-photon process for populating the $^1D_2$ multiplet.

In relation to the origin of the observed saturation power dependence, it should be considered that this effect is usually related to up-conversion processes depopulating one, or several, intermediate excited states in such a way that the up-conversion path becomes comparable or more probable than the relaxation paths to lower energy states. This produces a decrease in the slope obtained for those intermediate levels and, in consequence, in the slope of the levels populated from them.[37] Although transfer probabilities of Yb^{3+}-to-Tm^{3+} in YF_3 nanoparticles have not been reported yet, they have been obtained for YF_3 polycrystalline phosphors,[38] and show that the first energy transfer, that populates $^3H_5$ and $^3F_4$ levels of thulium, presents a lower probability than the next two consecutive transfer mechanisms, so that saturation effects seem to be highly probable.[32]

According to Fig. 6, since the different emission bands hold different power dependencies, the relationship between the bands and the colour of the emission can be modified by changing the excitation power. In that sense, higher powers produce an increase of blue and ultraviolet emissions in comparison to red emissions, and *vice versa*. Anyway, this is a slight modification compared to the changes that could be seen related to Tm^{3+} and Yb^{3+} contents, as it will be shown next.

Fig. 7 presents the emission spectra, after 975 nm excitation, of three samples with different Tm^{3+} content but the same Yb^{3+} concentration ([Yb^{3+}] = 10 mol%). With the aim of clearly comparing the obtained results, those spectra have been normalized dividing each one by the whole area of emission in the measured range. The emission spectra are strongly dependent on lanthanide ions concentration, as it can be deduced from the changes in the blue-to-red ratio of the emissions with thulium concentration. The figure includes also three pictures of those samples illustrating the change in colour that can be easily discerned by the naked eye. The photograph has been taken using a LUMIX digital camera with 1 s exposure at ISO 400. As it can be observed, the sample glows in a rather magenta hue, which oscillates from a reddish tone for the samples with higher thulium content and turns to a bluer tone when thulium content is diminished.

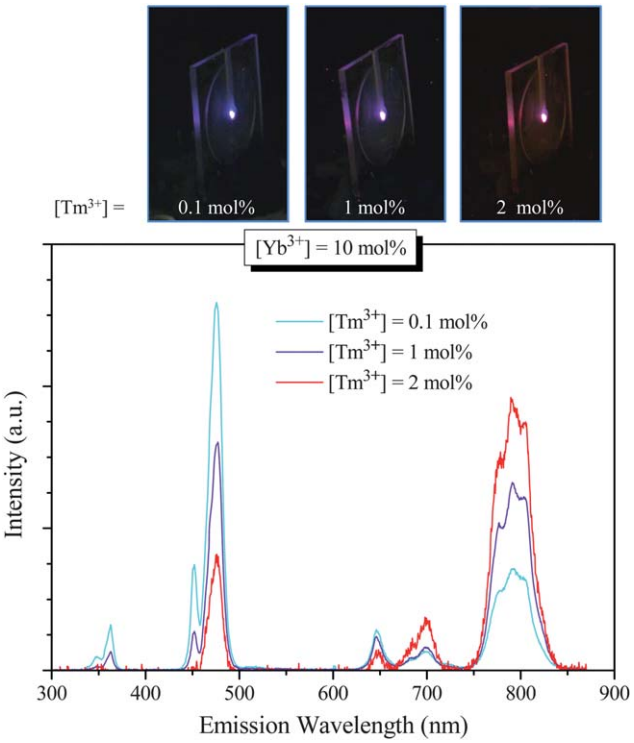

Fig. 7 Pictures of the emission of three samples with different doping content under the same excitation (up). The spectra obtained are shown in the graph. For comparison purposes they have been normalized to the whole emission area (down).

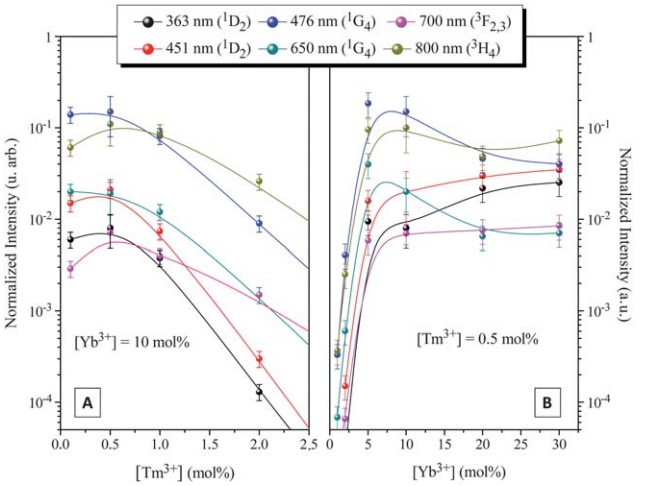

Fig. 8 Dependency of the intensity of the observed emission bands and doping concentrations keeping ytterbium (a) or thulium (b) content constant. The lines have been drawn to guide the eye.

To follow in detail the dependency between those colour changes and doping concentrations, two different series of samples have been synthesized. One of them keeps ytterbium concentration constant at $[Yb^{3+}] = 10$ mol%, while varies $[Tm^{3+}]$ concentration from 0.1 mol% up to 5 mol%. In the other one, on the contrary, thulium concentration has been kept constant at $[Tm^{3+}] = 0.5$ mol% while ytterbium content is changed from 1 mol% up to 30 mol%.

The luminescence spectra of these samples have been measured after 975 nm excitation keeping constant the excitation power (500 mW). The obtained results are similar to those presented in Fig. 7, except for the variation in the emission intensities of the different up-converted emissions. To quantify the results, the maximum peak emission of each band has been plotted *versus* doping concentration. The graphs can be seen in Fig. 8 for both concentration series (ytterbium constant Fig. 8a and thulium constant Fig. 8b). Each sample has been measured up to five times, removing it from the positioning platform and placing it back again on it to be sure that the measured changes in the bands are not caused by experimental artefacts. The error bars included in the figure correspond to an experimental uncertainty of around 20%, calculated from the average value of the different measurements. In addition, different groups of particles fabricated at the same time have been measured to guarantee the homogeneity of the samples. No observable changes have been obtained with that procedure.

As a first, general conclusion, it can be observed from Fig. 8 that luminescence intensities are strongly affected by the lanthanide ions content in the nanoparticles (note that the intensities are represented in a logarithmic scale, so that the variations cover several orders of magnitude). It appears also to be clear from the data that all the intensities are stronger at high ytterbium concentration (Fig. 8b), while they diminish with the increase of thulium content (Fig. 8a). In fact luminescence quenching by Tm^{3+} concentration is so strong that the emission becomes undetectable for the samples with higher thulium content ($[Tm^{3+}] = 5$ mol%).

The figure includes emissions at different wavelengths but originating from the same Tm^{3+} multiplet (363 nm and 451 nm, originating from the $^1D_2$ level, for instance) which, as expected, follow the same behaviour with doping concentration. This parallelism supports the reliability of the data.

Considering that the overall emission intensity is changing with dopant concentration, an alternative representation of the spectral changes in relation to the measured emission intensity is obtained normalizing the emissions to the intensity of the near infrared $^3H_4 \rightarrow {}^3H_6$ transition. That representation can be seen in Fig. 9, where the lines have been added to guide the eye.

As it can be seen, under that normalization, the intensity of the red emission, associated to $^3F_{2,3} \rightarrow {}^3H_6$ transition, holds a nearly constant value. This can be easily understood, considering that the $^3H_4$ energy level is populated from the decay of the $^3F_{2,3}$ upper-level and therefore their emissions are proportional to each other. The slight increase found, in the samples with constant thulium content ($[Tm^{3+}] = 0.5$ mol%), at the highest ytterbium concentrations, could be related to the effective UV-blue up-conversion processes that partially depopulate the $^3H_4$ level while keeps the $^3F_{2,3}$ population unaltered.

Regarding the UV and blue emissions, in samples with constant ytterbium concentration ($[Yb^{3+}] = 10$ mol%), it can be seen in Fig. 9a that their intensities, generated by the radiative decay from levels $^1D_2$ and $^1G_4$, decrease when Tm^{3+} concentration increases. On the other hand, in samples with constant thulium content ($[Tm^{3+}] = 0.5$ mol%), UV and blue emission bands show an initial increase with Yb^{3+} concentration, and their intensities remain dominant over the red emissions through the entire range of Yb^{3+} concentrations used in this work.

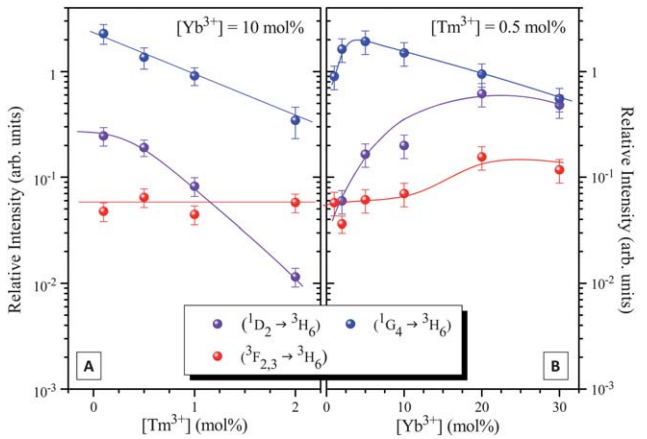

Fig. 9 Normalized intensities related to $^1D_2 \rightarrow {}^3H_6$ (purple dots), $^1G_4 \rightarrow {}^3H_6$ (blue dots) and $^3F_{2,3} \rightarrow {}^3H_6$ (red dots). The lines have been added to guide the eye.

It can be quantified by considering a blue to red ratio (BRR) calculated in terms of the area under the blue bands ($^1D_2 \rightarrow {}^3F_4$ and $^1G_4 \rightarrow {}^3H_6$) and the area related to the red bands ($^1G_4 \rightarrow {}^3H_6$ and $^3F_{2,3} \rightarrow {}^3H_6$) from emission spectra corrected for the response of the experimental set-up (monochromator and detector). These ratios change from a lowest value BRR $\approx$ 0.3 (reddish colour) to a highest value BRR $\approx$ 2 (bluish) for nanoparticles with concentrations changing from $[Yb^{3+}]$ = 10 mol%/$[Tm^{3+}]$ = 2 mol%, to $[Yb^{3+}]$ = 30 mol%/$[Tm^{3+}]$ = 0.5 mol%, respectively.

These emission changes associated to Yb^{3+} and Tm^{3+} concentrations can be understood, at least qualitatively, considering the UC-excitation mechanisms and the possible reverse processes (down-converting cross-relaxation processes or back-transfer mechanisms) that can take place in Yb^{3+}/Tm^{3+} doped materials. First, considering the multiphoton intrinsic nature of the up-conversion mechanisms, it is clear that increasing Yb^{3+} concentration (and Yb^{3+}/Tm^{3+} ratio) would facilitate the excitation of the upper Tm^{3+} multiplets. Also, it should be considered that several of the excited states of thulium may experience down-converting processes that will effectively quench Tm^{3+} emissions. In particular, it is well known that Tm^{3+} ions exhibit a highly effective infrared cross-relaxation process that depopulates the $^3H_4$ level, following the scheme $^2H_4 \rightarrow {}^3F_4$ (Tm^{3+}):$^3H_6 \rightarrow {}^3F_4$ (Tm^{3+}).[39–43] This process not only disrupts the sequence of up-conversion paths to populate the blue-emitting upper Tm^{3+} levels ($^1G_4$ and $^1D_2$) but it also simultaneously increases the population of the $^3F_4$ level, which feeds (by energy transfer from Yb^{3+}) the red emitting $^3F_{2,3}$ level (see Fig. 4). Therefore, this internal cross-relaxation process, which is enhanced by Tm^{3+} concentration, may contribute to the observed concentration dependencies.

Finally, in order to represent colour modifications in a quantitative way, the response of the standard human eye should be considered. For that reason, the CIE colour coordinates have been calculated, after correcting the spectra from the experimental response, and are shown in Fig. 10. In the figure, the arrows point towards the direction where doping concentration increases.

As it can be observed, the changes in the spectra produce different emission colours that go from a reddish hue ($[Yb^{3+}]$ = 10 mol%; $[Tm^{3+}]$ = 2 mol%) to a deep blue emission ($[Yb^{3+}]$ = 30 mol%; $[Tm^{3+}]$ = 0.5 mol%), covering several magenta hues in between.

Finally, it is also remarkable in Fig. 10 the opposite direction of the evolution of the hue with increasing concentrations of Tm^{3+} or Yb^{3+}. While higher thulium contents are related to reddish emissions, higher Yb^{3+} concentrations are connected to the bluest hues. Therefore, it can be said that the higher the Yb^{3+}/Tm^{3+} rate is, the highest population density will be found at thulium $^1G_4$ and $^1D_2$ energy levels and the bluest the emission will be.

Conclusions

YF_3:Tm^{3+}/Yb^{3+} nanocrystals, with variable concentrations, have been synthesized and optically analysed. It has been found that

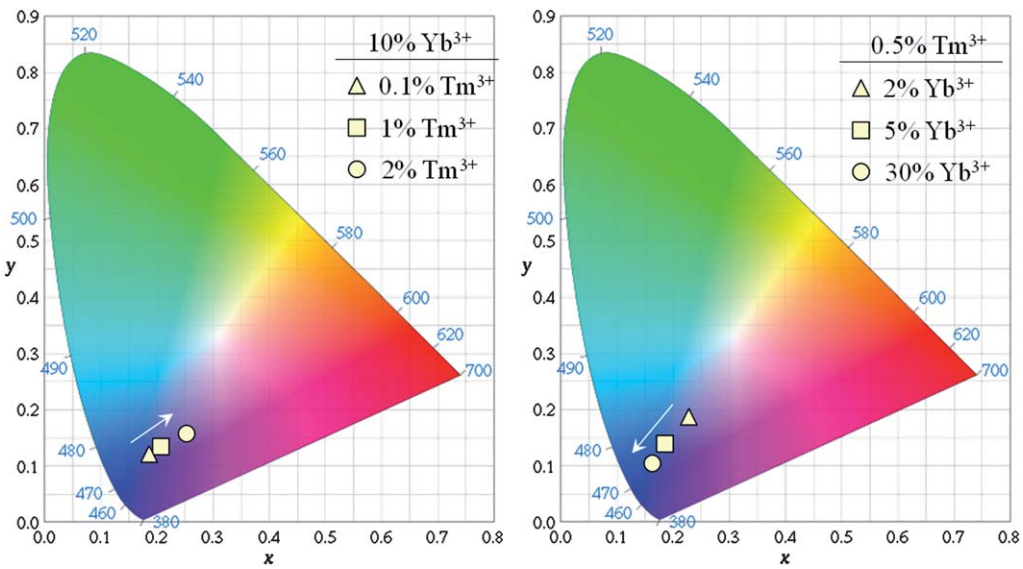

Fig. 10 CIE colour coordinates of three different samples of each concentration series, $[Yb^{3+}]$ constant (left) and $[Tm^{3+}]$ constant (right).

the emission hue is strongly dependent on the concentration of the doping ions. The gradual changes obtained have been studied, finding that high Tm^{3+} and low Yb^{3+} contents enhance red emissions, while low Tm^{3+} and high Yb^{3+} can be associated to dominant blue light. Selecting the adequate lanthanide ions concentrations it is possible to selectively tune the overall emission within different shades of magenta emissions.

Acknowledgements

This work has been partially supported by the spanish Ministerio de Ciencia e Innovación (MICINN) (projects CRONOSOMATS (MAT2009-14102) and MAT2008-02166), by Comunidad de Madrid (project MICROSERES-CM (S2009/TIC-1476)), and by Junta de Andalucía (grant FQM3579). Additionally, N. O. Nuñez wants to thank the spanish Ministerio de Ciencia e Innovación (MICINN) and the Spanish Research Council (CSIC) for her financial support (PIE-200960I127).

References

1 A. Rapaport, J. Milliez, M. Bass, A. Cassanho and H. Jenssen, *J. Disp. Technol.*, 2006, **2**, 68–78.
2 R. Scheps, *Prog. Quantum Electron.*, 1996, **20**, 271–358.
3 E. Downing, L. Hesselink, J. Ralston and R. Macfarlane, *Science*, 1996, **273**, 1185–1189.
4 D. K. Chatterjee, A. J. Rufaihah and Y. Zhang, *Biomaterials*, 2008, **29**, 937–943.
5 M. Nyk, R. Kumar, T. Y. Ohulchanskyy, E. J. Bergey and P. N. Prasad, *Nano Lett.*, 2008, **8**, 3834–3838.
6 Z. Tian, G. Y. Chen, X. Li, H. J. Liang, Y. S. Li, Z. G. Zhang and Y. Tian, *Lasers Med. Sci.*, 2010, **25**, 479–484.
7 G. Y. Chen, T. Y. Ohulchanskyy, R. Kumar, H. Agren and P. N. Prasad, *ACS Nano*, 2010, **4**, 3163–3168.
8 A. M. Smith, M. C. Mancini and S. Nie, *Nat. Nanotechnol.*, 2009, **4**, 710–711.
9 M. Gu, *Advanced Optical Imaging Theory*, Springer-Verlag, Berlín, Heidelberg, Alemania, 2000.
10 M. Antonietti, D. Kuang, B. Smarlsy and Y. Zhou, *Angew. Chem., Int. Ed.*, 2004, **43**, 4988–4992.
11 M. A. Klingshirn, S. K. Spear, J. D. Holbrey and R. D. Rogers, *J. Mater. Chem.*, 2005, **15**, 5174–5180.
12 A. Bril, J. L. Sommerdijk and A. W. de Jager, *J. Electrochem. Soc.*, 1975, **122**, 660–663.
13 M. M. Lage, A. Righi, F. M. Matinaga, J. Y. Gesland and R. L. Moreira, *J. Phys.: Condens. Matter*, 2004, **16**, 3207–3218.
14 G. S. Yi and G. M. Chow, *J. Mater. Chem.*, 2005, **15**, 4460–4464.
15 N. O. Núñez and M. Ocaña, *Nanotechnology*, 2007, **18**, 455606.
16 V. Mahalingam, F. Vetrone, R. Naccache, A. Speghini and J. A. Capobianco, *Adv. Mater.*, 2009, **21**, 4025–4028.
17 G. F. Wang, W. P. Qin, J. Zhang, J. S. Zhang, Y. Wang, C. Y. Cao, L. L. Wang, G. D. Wei, P. Zhu and R. J. Kim, *J. Phys. Chem. C*, 2008, **112**, 12161–12167.
18 M. Wang, Q. L. Huang, H. X. Zhong, X. T. Chen, Z. L. Xue and X. Z. You, *Cryst. Growth Des.*, 2007, **7**, 2106–2111.
19 A. Yin, Y. Zhang, L. D. Sun and C. H. Yan, *Nanoscale*, 2010, **2**, 953–959.
20 J. Shan, M. Uddi, R. Wei, N. Yao and Y. G. Ju, *J. Phys. Chem. C*, 2010, **114**, 2452–2461.
21 G. F. Wang, W. P. Qin, L. L. Wang, G. D. Wei, P. Zhu and R. J. Kim, *Opt. Express*, 2008, **16**, 11907–11914.
22 K. W. Krämer, D. Biner, G. Frei, H. U. Güdel, M. P. Hehlen and S. R. Lüthi, *Chem. Mater.*, 2004, **16**, 1244–1251.
23 G. De, W. P. Qin, J. S. Zhang, J. S. Zhang, Y. Wang, C. Y. Cao and Y. Cui, *J. Lumin.*, 2007, **122–123**, 128–130.
24 C. Y. Cao, W. P. Qin, J. S. Zhang, Y. Wang, P. Zhu, G. F. Wang, G. D. Wei, L. L. Wang and L. Z. Jin, *J. Fluorine Chem.*, 2008, **129**, 204–209.
25 G. F. Wang, W. P. Qin, L. L. Wang, G. D. Wei, P. Zhu, D. S. Zhang and F. H. Ding, *J. Rare Earths*, 2009, **27**, 330–333.
26 D. Q. Chen, Y. S. Wang, Y. L. Yu and P. Huang, *Appl. Phys. Lett.*, 2007, **91**, 051920.
27 G. F. Wang, W. P. Qin, G. D. Wei, L. L. Wang, P. Zhu, R. J. Kim, D. S. Zhang, F. H. Ding and K. Z. Zheng, *J. Fluorine Chem.*, 2009, **130**, 158–161.
28 C. Y. Cao, W. P. Qin and J. S. Zhang, *J. Nanosci. Nanotechnol.*, 2010, **10**, 1900–1903.
29 W. P. Qin, D. S. Zhang, D. Zhao, L. L. Wang and K. Z. Zheng, *Chem. Commun.*, 2010, **46**, 2304–2306.
30 N. O. Núñez, M. Quintanilla, E. Cantelar, F. Cussó and M. Ocaña, *J. Nanopart. Res.*, 2010, **12**, 2553–2565.
31 *Handbook of Chemistry and Physics*, ed. D. R. Lide, CRC Press, Boston, 72nd edn, 1991–1992.
32 J. E. Geusic, F. W. Ostermayer, H. M. Marcos, L. G. van Uitert and J. P. van der Ziel, *J. Appl. Phys.*, 1971, **42**, 1958–1960.
33 F. Auzel, *C. R. Acad. Sci. (Paris)*, 1966, **263**, 819–821.
34 R. A. Hewes and J. F. Sarver, *Phys. Rev.*, 1969, **182**, 427–436.
35 S. Heer, K. Kömpe, H.-U. Güdel and M. Haase, *Adv. Mater.*, 2004, **16**, 2102–2105.
36 J. F. Suyver, J. Grimm, M. K. van Veen, D. Biner, K. W. Krämer and H. U. Güdel, *J. Lumin.*, 2006, **117**, 1–12.
37 M. Pollnau, D. R. Gamelin, S. R. Lüthi, H. U. Güdel and M. P. Hehlen, *Phys. Rev. B: Condens. Matter Mater. Phys.*, 2000, **61**, 3337–3346.
38 F. W. Ostermayer, J. P. van der Ziel, H. M. Marcos, L. G. van Uitert and J. E. Geusic, *Phys. Rev. B: Solid State*, 1971, **3**, 2698–2705.
39 M. Quintanilla, E. Cantelar, J. A. Sanz-García, G. Lifante, G. A. Torchia and F. Cussó, *J. Lumin.*, 2008, **128**, 927–930.
40 A. Brenier, C. Pedrini and B. Moine, *Phys. Rev. B: Condens. Matter*, 1990, **41**, 5364–5371.
41 F. Güell, J. Gavaldà, R. Solé, M. Aguiló, F. Díaz, M. Galán and J. Massons, *J. Appl. Phys.*, 2004, **95**, 919–923.
42 H. Hayashi, S. Tanabe and T. Hanada, *J. Appl. Phys.*, 2001, **89**, 1041–1045.
43 Y. S. Han, J. H. Song and J. Heo, *J. Appl. Phys.*, 2003, **94**, 2817–2820.

